Advanced Functional Materials

ADVANCED FUNCTIONAL MATERIALS
www.afm-journal.de

RESEARCH ARTICLE OPEN ACCESS

Photo-Degradable Polyester Networks and Multi-Photon Printed Objects Based on Cyclic Ketene Acetals

Till Meissner[1,2,3] | Julian Fanelli[3] | Vinh Xuan Truong[4] | Rob Jones[5] | Jens Gaitzsch[1,2] | Christopher Barner-Kowollik[3,6]

[1]Leibniz-Insitute of Polymer Research Dresden e.V. (IPF), Dresden, Saxony, Germany | [2]Faculty of Chemistry and Food Chemistry, Organic Chemistry of Polymers, Dresden University of Technology (TUD), Dresden, Saxony, Germany | [3]School of Chemistry and Physics, Centre for Materials Science, Queensland University of Technology (QUT), Brisbane, Queensland, Australia | [4]Institute of Sustainability for Chemicals, Energy and Environment (ISCE2), Agency for Science, Technology and Research (A*STAR), Singapore, Singapore | [5]Central Analytical Research Facility, Queensland University of Technology (QUT), Brisbane, Queensland, Australia | [6]Institute of Functional Interfaces (IFG), Karlsruhe Institute of Technology (KIT), Eggenstein-Leopoldshafen, Baden-Württemberg, Germany

Correspondence: Jens Gaitzsch (gaitzsch@ipfdd.de) | Christopher Barner-Kowollik (christopher.barnerkowollik@qut.edu.au)

Received: 30 June 2026 | **Revised:** 17 August 2026 | **Accepted:** 1 September 2026

Keywords: cyclic ketene acetals | multi-photon printing | pyrene chalcones | radical ring-opening polymerization | reversible photocycloaddition | selective erasure

ABSTRACT

Radical ring-opening polymerization (RROP) of cyclic ketene acetals (CKAs) constitutes a powerful avenue to biodegradable polyesters via radical polymerization. CKA-based degradable polymers have been established mainly as linear polymers, while networks from CKA-based RROP remain scarce despite their potential as degradable materials. Herein, a photoreversible RROP-polyester network based on poly(2-methylene-1,3,6-trioxocane) (PMTC) is introduced. Photoreversibility is achieved by decorating the PMTC chains with pendant pyrene chalcone (PyChal) moieties. Photoinduced [2+2] cycloaddition (λ_{max} = 440 nm) of the PyChal moieties affords covalent cross-links, while irradiation at λ_{max} = 345 nm allows for network reversion as underpinned by an in-depth solution assessment of the photochemistry. The reversible nature of the photochemistry enables repeatable gel-sol transitions as shown by variations in their storage and loss modulus (resulting in *G*' changes of up to 9 kPa). Importantly, the photoreactive CKA-based polymer can be employed in light-driven multi-photon printing (MPP) without the need for any initiators, allowing the fabrication of pre-determined spatially confined architectures as evidenced by ToF-SIMS. The MPP structures can be degraded by expore to UV irradiation and alkaline conditions. We thus establish a degradable PCKA-based resist with reversible photochemistry for modular soft matter manufacturing.

1 | Introduction

The ubiquity of non-degradable polymer materials has produced a well-documented environmental crisis: persistent plastic waste, fragmentation into micro- and nano-plastics, and associated ecological and human-health impacts are now recognized as major global challenges [1–3]. Continued growth in plastic production and insufficient waste management have driven increased attention to polymer designs that enable controlled degradation or–ideally–circular lifecycles. Within this context, aliphatic polyesters have emerged as an appealing route toward degradable materials, which has prompted significant research interest over the last decades [4–7]. Conventional polyesters are prepared via polycondensation of bifunctional monomers or ring-opening polymerization (ROP) of cyclic monomers [8]. While ROP offers excellent control over polymer architecture and

molecular weight, it commonly relies on catalytic systems and highly purified monomers, whereas conventional lactone-derived polyesters generally lack readily accessible pendant functional groups. Consequently, introducing functionality often requires either elaborate monomer synthesis prior to polymerization or post-polymerization modification through additional synthetic steps that can compromise the integrity of the polyester backbone, thereby limiting the versatility of these materials. In contrast, radical ring-opening polymerization (RROP) of cyclic ketene acetals (CKAs) has emerged as a powerful alternative, combining the synthetic robustness and broad tolerance towards functional groups of free-radical polymerization with the ability to generate degradable polyester backbones. RROP of CKAs hence provides a straightforward route towards functional, biocompatible, and biodegradable aliphatic polyesters, while overcoming several limitations associated with conventional ROP [9–12].

Pioneered by Bailey et al. in 1982, the synthesis of polyesters via RROP of CKAs – referred to as poly(CKAs) (PCKAs) – fuses advantageous features of free-radical polymerization (FRP) as well as ring-opening polymerization, i.e. robust reaction conditions from FRP coupled with ester functionalities through ROP [13–15]. Inherently, compared with PCL-based systems, PCKA materials offer several advantages, including their innate propensity for branching during RROP, which can be used to tailor the polyester microstructure. Furthermore, linear PCKAs have previously been demonstrated to undergo enzymatic degradation, where the semi-crystallinity (=the microstructure) affects the degradation rate, representing an advantage that may be exploited in future studies. Over the past decades, a range of CKAs have been developed ranging from hydrophilic [16, 17], amine-bearing [10, 11, 18], to unsaturated [19] and circularly-operated derivatives [20–23], and their propensity to undergo RROP has been explored in-depth [24–27]. These studies demonstrate that RROP unlocks tunable ester content, molecular architecture, and degradation susceptibility across homo- and copolymers.

Despite these advances, the majority of research on PCKAs has been directed towards thermoplastic polyester architectures, while cross-linked polymer networks are explored to a lesser extent. 3D scaffolds have been reported to include PCKAs as a minor component to achieve degradability into (meth)acrylic networks in a variety of contexts, mostly focusing on 2-methylene-1,3-dioxepane (MDO) and 2-methylene-1,3,6-trioxocane (MTC) as CKAs. Such materials have been used in a wide range of applications, including thermo-responsive networks [28–31], amphiphilic gels [32], networks for biomedicine (e.g., tissue engineering [33, 34], or drug delivery [35]), bioelastomers [36], biomimetics [37] and robust tissue adhesives [38–42]. In these studies, the responsive behavior relied on temperature, pH or an enzymatic gradient as stimulus to trigger a specific response. In contrast, the use of light as a traceless reagent offers key benefits due to its non-invasiveness and spatiotemporal precision [43], which has also been exploited in vinylic networks with CKAs as a minor component. For instance, Agarwal and colleagues reported a network with pendant coumarin groups which were photocross-linked at 365 nm into amphiphilic micelles and subsequently photochemically reverted upon irradiation with high-energy 254 nm UV light [35]. Similarly, Xie et al. developed a copolymer-network with pendant coumarin entities that yielded mechanically stable, antimicrobial adhesives upon UV-induced cross-linking [42]. Advancing beyond coumarins, Gorman and co-workers incorporated benzophenone moieties into the side chain to generate antibiofouling films by means of a UV-induced covalent bond formation [41]. The group of Carlotti took the utilization of light further and developed a photoresist formulation for additive and subtractive manufacturing via two-photon printing (2PP), enabling the fabrication of a plethora of hydrolyzable arbitrary structures with high fidelity [44]. Despite these important contributions, networks that are primarily composed of PCKAs and fuse reversible light-responsiveness with intrinsic degradability have not yet been realized. 3D-printed microstructures capable of reversible photomodulation in combination with the ability for chemical or photolytic degradation thus present a critical research gap.

We herein report a dual degradable network based on PMTC copolymerized with a vinyl comonomer, bearing pendant pyrene chalcone (PyChal) units as minor component. PyChal units can be subjected to a reversible light-induced [2+2] cycloaddition for network formation and UV-triggered cycloreversion for network degradation. We examine the photochemical behavior of these materials in solution as well as in the bulk state using photorheology to demonstrate photoreversibility. Once established, our system serves as the basis for a photoresist based on our PCKA-PyChal system for multi-photon printing (MPP) to unlock the fabrication of three-dimensional structures which are inherently susceptible to basic, enzymatic as well as light-induced degradation pathways. Our work establishes a general strategy for degradable RROP-polyester networks compatible with advanced and reversible photo-manufacturing as well as sustainable materials design.

Importantly, the current study significantly expands RROP of CKAs to provide an avenue towards photo-decomposable and hydrolyzable network materials constituting of PMTC-PyChal. We initially copolymerize the CKA (MTC) with 2-chloroethyl vinyl ether (CEVE) to synthesize copolymers with pending functional groups. We selected MTC as the CKA building block for the polymer backbone due to its pronounced ring-opening propensity and favorable reactivity under diverse radical polymerization conditions, enabling the formation of non-cross-linked polyesters [45]. MTC belongs to a broader class of synthetically accessible CKAs, including MDO, BMDO and MPDL, which can be prepared via the well-established haloacetal route in a concise two-step procedure and on multigram scale [45]. The increasing commercial availability of CKAs, including MTC, further facilitates access to these monomeric building blocks and highlights the growing practical maturity of CKA chemistry for the synthesis of degradable polyesters [24, 46]. In a post-polymerization protocol, we decorate the vinylic units within the PCKA backbone with pendant PyChal entities by means of a copper(I)-catalyzed azide-alkyne cycloaddition (CuAAC) (Scheme 1A). Our modular strategy exploits the pendant vinyl ether (VE)-derived functionality introduced directly during the statistical RROP of CKAs and VEs, thereby avoiding the need for elaborate synthesis of functionalized (lactone) monomers, while preserving the integrity of the degradable polyester backbone. Notably, the complete synthetic sequence, including the PPF protocol, can be reliably performed on the gram scale, demonstrating the overall amenability to scale-up. We subsequently establish the photochemistry of these materials in solution (sol-state)

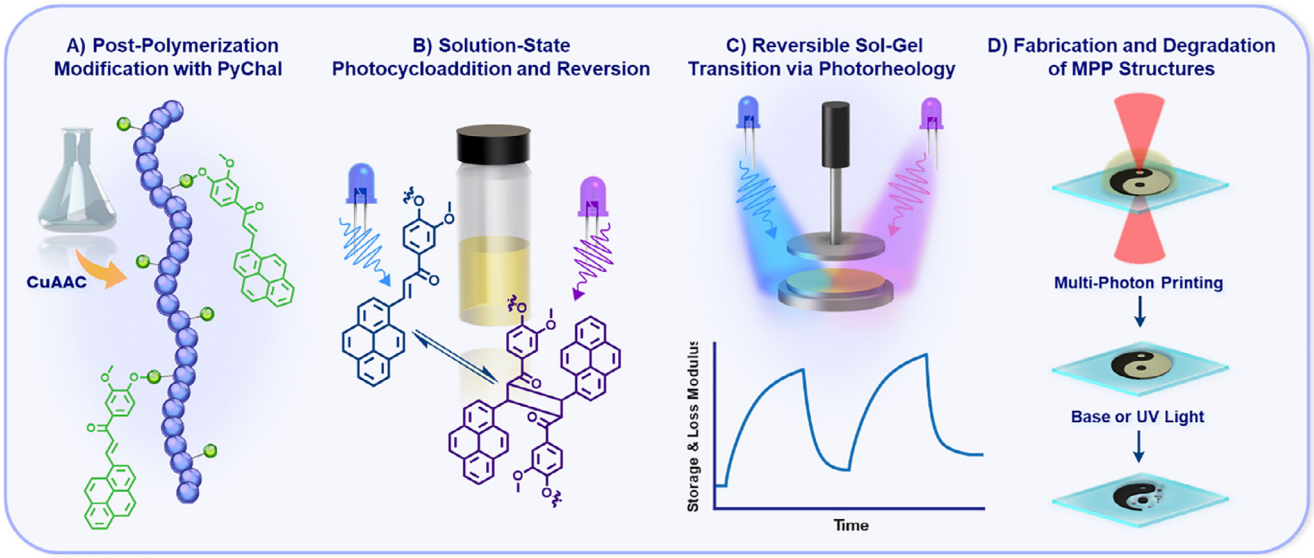

SCHEME 1 | Overview of the current study. (A Synthesis of P(MTC-*co*-PyChalEVE) via post-polymerization-functionalization. (B) Exploration of copolymer photochemistry via solution-state studies. (C) Photoreversibility of material properties via photorheological assessment. (D) Multi-photon printing of P(MTC-*co*-PyChalEVE) and degradation through multiple stimuli.

using combined UV/Vis and NMR spectroscopy, size exclusion chromatography (SEC) and LC-MS characterization. After demonstrating photoreversibility (Scheme 1B), the networks are studied by photorheology, demonstrating that the material properties can be modulated by different colors of light (Scheme 1C). Finally, we employ our photoreactive polymer to formulate a P(CKA-*co*-PyChal) photoresist, which enables the manufacturing of 3D-printed microstructures through MPP (Scheme 1D) [47, 48]. Subsequent degradation via either light or base hydrolysis proves the multimodal degradability of the generated structures. These findings underscore the versatility of PCKAs and will incentivize their use in advanced contemporary fields of application.

2 | Results and Discussion

To enable PCKAs for photochemical network formation, we selected [2+2]-photocycloaddition as the cross-linking chemistry, as it affords efficient covalent bond formation that can be reversibly gated by different colors of light [49]. Specifically, we employ PyChal as a visible light-responsive chromophore owing to its superior synthetic scalability as well as tunable functionality opposed to, for instance, styrylpyrenes [50–53]. In addition, photocycloaddition as well as reversion of the PyChal system can be triggered with red-shifted, more benign wavelengths important for potential biological applications [53]. Initial attempts to incorporate PyChal directly into an aliphatic polyester via copolymerization with MTC were unsuccessful. VE and methyl methacrylate (MMA) derivatives of PyChal either failed to copolymerize (Scheme S1 and Figure S3) or underwent undesired side reactions. The highly reactive intermediate primary radical present during the polymerization of MTC attacked the chalcone double bond, resulting in premature termination and chromophore deconjugation (Figure S4). These results are consistent with previous reports on PyChal demonstrating that free-radical polymerization of chalcone moieties succeeds preferentially when adjacent groups stabilize intermediate radicals (e.g. methacrylate-based chalcone) [54–57]. Attempts to mask the chalcone double bonds by prior photocycloaddition and subsequent immediate network formation via bisfunctional PyChal dimers also proved ineffective. We attribute this to either a lack of reactivity (VE derivatives) or mismatched reactivity ratios (MMA derivative). Collectively, these findings motivated a strategy based on the post-polymerization functionalization (PPF) of a prefabricated PMTC backbone bearing VE repeat units. Grafting-from will allow for attaching the PyChal units after the backbone has been synthesized. MTC was chosen as PCKA due to its superior reactivity during RROP as well as its tendency to form completely ring-opened polyesters [45]. In order to include the PyChal moiety, we adapted a synthetic procedure reported by Guillaneuf and colleagues, who exploited similar reactivity ratios between MTC/MDO and functional VEs in free-radical copolymerizations [36, 58]. Based on their protocol, MTC was copolymerized with CEVE, and the PyChal handles introduced using CuAAC (Scheme 2) [59]. CuAAC is known for its high functional group tolerance, selectivity and benign reaction conditions and has been shown to tolerate chalcone moieties and the labile polyester backbone in a variety of instances [36, 59–61].

As the initial step of the synthetic sequence, MTC was copolymerized with CEVE (F_{MTC}:F_{CEVE} = 84:16) at 70°C in the presence of 2,2'-azobis(2-methylpropionitrile) (AIBN, 1 mol%) as a radical initiator in bulk (refer to Scheme S2). The resulting P(MTC-*co*-CEVE) was isolated and characterized by ^{1}H-NMR spectroscopy as well as SEC. Initial kinetic experiments at the targeted feed ratio reveal a modest compositional drift toward higher CEVE incorporation (F_{CEVE} >20%) and a pronounced loss of molar mass control (formation of ultra-high molar mass species) over extended reaction times (after 24 h, refer to Figure S9). Note that the dispersity ($Đ$) also increased from 2.9 to 56 at longer reaction times owing to the tendency of MTC/PMTC to undergo chain transfer reactions under radical conditions, leading to a significantly increased $Đ$ [62, 63]. To balance conversion and compositional drift, reactions were quenched at a conversion

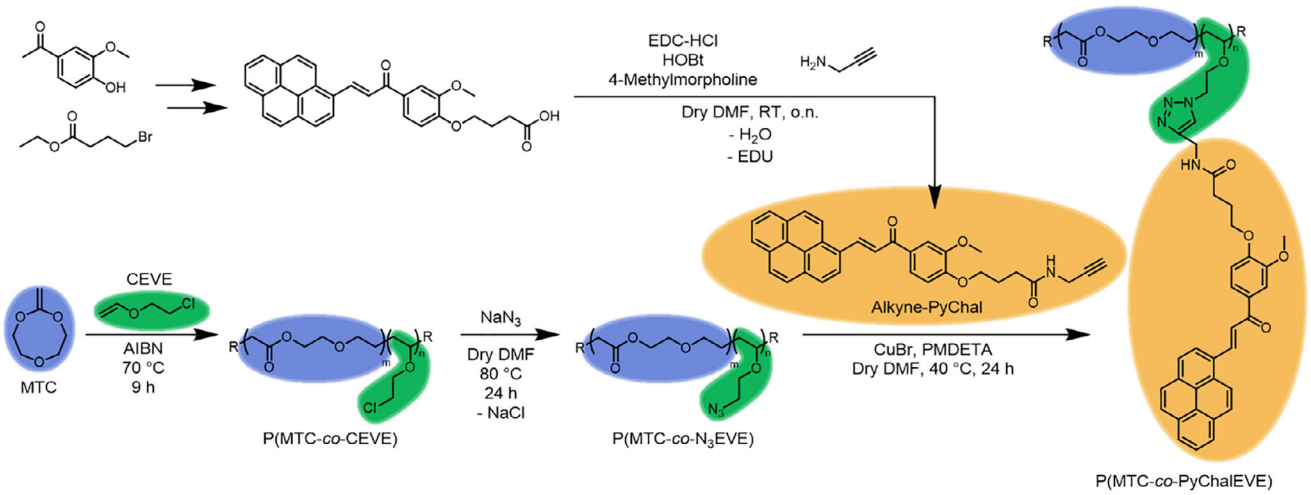

SCHEME 2 | Synthetic sequence toward PyChal-decorated polyester P(MTC-*co*-PyChalEVE) via copolymerization and subsequent post-polymerization-functionalization.

of 65%–70%, preserving both the feed composition and molar mass control. After optimization (reaction quenched after 9 h), P(MTC-*co*-CEVE) was obtained with good retention of the initial co-monomer feed as evidenced by ^{1}H-NMR ($F_{MTC} = 84\pm 4$, $F_{CEVE} = 16\pm 4$, Figure S5), an M_n of close to 9000 g mol^{-1} and $Đ$ of 2.9 (Figure S8, refer to the Supporting Information S1: Section 2.2.2.1 for details of molar ratio as well as functional group density determination) [36]. As PCKAs are prone to undergo branching reactions, the density of branching (DB) had to be evaluated. It was determined to be 7.3% via ^{1}H-NMR spectroscopy, that is, 4–5 PMTC repeating units per chain showed short- or long-chain branching. This value is notably lower than for PMTC homopolymers, implying a more defined polymeric architecture [62, 63]. In agreement with previous studies, ^{13}C-NMR spectroscopy showed no ring-retained MTC, suggesting quantitative ring-opening toward the aliphatic polyester (refer to Figure S6) [63–65]. The microstructure of the copolymer was determined by 2D NMR analyses, revealing the presence of various dyads, confirming the copolymerization reaction (refer to Figure S7). The absence of larger CEVE blocks was further evidenced by SEC-MS in combination with degradative studies. Complete disintegration of the pristine polymer upon basic degradation was shown by NMR spectroscopy, SEC and SEC-MS (refer to Figures S11–S15 and Tables S3 and S4). Somewhat surprisingly, the THF-SEC trace of the purified copolymer was distinctly bimodal (refer to Figures S8 and S10). When the eluent was changed from THF to DMAc, the populations merged (refer to Figure S10), indicating that secondary interactions with the SEC column likely caused the THF-SEC elution behavior, rather than intrinsic chemical heterogeneity. Together these results emphasize that the polymer exhibits a unimodal distribution [66]. This finding is consistent with that reported by Guillaneuf and coworkers, who observed near-ideal reactivity ratios for VEs (including CEVE) and MTC/MDO together with little to no multimodality in SEC [36, 58, 67].

After successful introduction of functional handles into the polyester backbone, the pendant alkyl chloride moieties were converted to azides via nucleophilic substitution using sodium azide (refer to Scheme S3) [36]. Quantitative conversion was achieved after 24 h at 80°C unlocking P(MTC-*co*-N$_3$EVE) (refer to Figure S16, refer to the Supporting Information S1: Section 2.2.2.2 for details of molar ratio as well as functional group density determination). The first step of PPF was accompanied by a slight decrease in molar mass (M_n = 7500 g mol^{-1}; $Đ$ = 2.9), but under retention of the MTC/VE ratio, suggesting negligible polyester backbone degradation during azide-functionalization (refer to Figure S17). The complementary alkyne-bearing PyChal reagent was prepared from its accessible acid precursor following a reported procedure [53]. Capitalizing on the carboxylic acid moiety, EDC/HOBt-mediated amidation with propargylamine and 4-methyl morpholine was performed at ambient temperature overnight, affording the respective alkyne-PyChal in excellent yield and purity (refer to Scheme S4 + Figures S18–S21). With both the azide-functional polymer and alkyne-PyChal at hand, CuAAC was performed in the presence of Cu(I)Br as well as PMDETA at 40°C for 24 h (refer to Scheme S5). Purification by preparative SEC and subsequent precipitation afforded the final P(MTC-*co*-PyChalEVE). We acknowledge that preparative SEC is not routinely available as a polymer purification technique. The extended polyaromatic structure of PyChal, together with its limited solubility in solvents compatible with conventional precipitation and dialysis, renders these more broadly accessible purification approaches comparatively inefficient and solvent intensive. In addition, strong aromatic interactions may promote retention or physical retaining of residual low-molecular-weight PyChal within the precipitated polymer, potentially complicating the reliable assessment of chromophore incorporation. We therefore employed SEC, which separates species according to their hydrodynamic size rather than polarity and is particularly well-suited to the pronounced size difference between the free PyChal chromophore and the corresponding PyChal-functionalized PCKA. The purification procedure was performed on the gram scale, affording up to 1.5 g of the final P(MTC-*co*-PyChalEVE) with an isolated yield of approximately 70% (see Supporting Information S1: Section 1.4 for detailed purification procedures and SEC specifications). Thus, despite its comparatively limited accessibility, preparative SEC provided an efficient means of removing excess low-molecular-weight PyChal on a preparatively relevant scale without substantial loss of polymer.

More accessible alternatives could include solid-phase covalent scavenging using azide-functionalized silica to selectively remove residual alkyne-bearing PyChal via CuAAC, or Soxhlet extraction to remove low-molecular-weight species. ^{1}H-NMR spectroscopy indicated good preservation of the initial molar composition of the copolymer, accompanied by quantitative disappearance of the azide-associated resonances. The emergence of the triazole proton in the aromatic region, together with broadened PyChal proton resonances, also indicated the successful ligation (Figure S22, refer to Supporting Information S1: Section 2.2.2.4 for details of molar ratio as well as functional group density determination). Exclusion of low molar mass fractions during preparative SEC shifted the observed molar mass distribution toward a higher M_n of close to 12 600 g mol^{-1} and slightly lower $Đ$ of 2.6 while bearing a unimodal size population (refer to Figure S23). Dual DRI/UV (λ = 420 nm) detection indicated coinciding signals, confirming ligation of PyChal to the polymer backbone, which itself is UV-transparent at this wavelength. UV/Vis spectroscopy in DMF displayed the characteristic PyChal absorbance in its conjugated state, thus demonstrating the successful preservation of the pristine structure of this moiety (refer to Figure S24).

After the successful synthesis of the PyChal-decorated PCKA, we monitored the photo-induced network formation and degradation by means of solution-state techniques, such as NMR- and UV/Vis spectroscopy and SEC. Experiments were thus conducted at copolymer concentrations sufficiently low to form sols rather than gels. Preliminary experiments at a PyChal concentration of 7 wt.% (66.3 mM, corresponding to 6.61 mM copolymer) resulted in solidification of the sample upon blue-light irradiation. Accordingly, lower concentrations were employed to prevent complete gelation while enabling the photo-induced dimerization and subsequent cycloreversion to be monitored under liquid-state conditions. To gain a chemical understanding of the photo-induced dimerization and its reversion, a series of ^{1}H-NMR spectra were recorded with a 2.5 wt.% PyChal (18.3 mM corresponding to 1.83 mM copolymer) concentration in DMSO-d_6. The yellow solution comprising P(MTC-*co*-PyChalEVE) was illuminated with a λ_{max} = 440 nm LED (I = 294 mW cm^{-2}) for 5 min, yielding a noticeably paler yellow mixture. This color of light was chosen as PyChal exhibits its highest reactivity in that wavelength regime [68]. Upon irradiation, broad resonances emerged in the ^{1}H-NMR spectrum at δ = 5.25 ppm (light orange tile in Figure 1A,B) corresponding to the characteristic cyclobutane protons formed via [2+2]-photocycloaddition of the PyChal units. At the same time, the integral of the resonance associated with the olefinic protons of PyChal at δ = 8.75 ppm (light blue tile in Figure 1A,B) decreased accordingly. This change in chemical environment also prompted the chalcone proton at δ = 7.10 ppm to shift to δ = 6.80 ppm (red tile in Figure 1A,B). Based on this change, we estimate the degree of dimerization by comparing the integral intensity of the cyclobutane protons (δ = 5.25 ppm) to an internal standard (PMTC methylene backbone at δ = 4.10 ppm; indigo tile in Figure 1A,B). The chalcone proton at δ = 7.10 ppm was used to define the upper limit for the cyclobutane integral (red tile in Figure 1A,B; refer to Figure S25 and Table S5 for detailed explanation and calculation). Following this approach, a dimer content of close to 88% was calculated after 5 min of λ_{max} = 440 nm irradiation. Subsequent exposure to UV light of λ_{max} = 310 nm (I = 38 mW cm^{-2}) triggered photocycloreversion of the PyChal adducts: The cyclobutane integral decreased progressively, reaching a reversion of close to 60% after 120 min (i.e., close to 40% dimer remained). Prolonged irradiation did not increase reversion, consistent with the establishment of a photostationary state at λ_{max} = 310 nm in which cycloaddition and reversion progress at the same rate [68, 69]. In agreement with photocycloreversion, distinct sharp resonances emerged in the aromatic region, indicative of small-molecule formation (dark orange tile in Figure 1A,B). These resonances are associated with the asymmetric cleavage product during photocycloreversion–bispyrene (molecule highlighted in turquoise in Figure 1A) [49]. LC-MS analysis confirmed the presence of a species with m/z = 428.16, whose mass and isotope pattern match $C_{34}H_{20}$ (bispyrene, refer to Figure S26C + D). The MS evidence is consistent with the detection of bispyrene as a radical cation rather than a protonated ion as no mass alteration is observed. Such a behavior fits a previously reported pattern for large, highly conjugated systems that are difficult to ionize by ESI [70]. In addition, the photodiode array (PDA) UV/Vis spectrum of this species revealed a red-shifted absorbance compared to PyChal, congruent with the extended, conjugated π-system of bispyrene (refer to Figure S26E) [71].

To evaluate the aforementioned light-induced network formation and reversion, we conducted a series of UV/Vis spectroscopy measurements of an 18.3 mM PyChal (1.83 mM copolymer) solution in DMAc as optical readout of these photochemistries. The solution initially displayed absorption extending into the blue regime (λ = 420 nm), characteristic of the conjugated PyChal chromophore (red trace in Figure 1C). Irradiation at λ_{max} = 440 nm caused a pronounced decrease of this long-wavelength band and the concurrent appearance of a blue-shifted doublet at approx. λ = 330 and 350 nm, indicating the formation of pyrene-derived photoadducts arising from disruption of the pristine conjugation [53]. The wavelength at which the absorbances of photoactive species account for the same value (isosbestic point) was found at λ = 359 nm and remained unchanged, demonstrating selective formation of the photoadduct. In order to demonstrate the photocycloreversibility under lower-energy irradiation conditions, we opted for an LED with λ_{max} = 345 nm (I = 13 mW cm^{-2}). Illumination at that wavelength progressively reduced the pyrene-associated bands, while the red-shifted absorbance increased again (dashed traces in Figure 1C). Based on identical aliquots taken from the reaction mixture at each time point (equivalent concentration allowing for quantification via absorbance), the absorbance at λ = 409 nm recovered close to 60% of the initial value after 120 min exposure at λ_{max} = 345 nm. Note that this recovery solely reflects the photocycloreversion of the cyclobutane adduct rather than regeneration of the initial PyChal entity. The cycloreversion is supported by a shift in the isosbestic point from λ = 359 nm to shorter wavelengths, further indicating a drift from a binary to a multicomponent photoactive mixture over extended λ_{max} = 345 nm irradiation [51]. These observations are consistent with the formation of asymmetric cleavage products (e.g., bispyrene, refer to Figure S26), whose extended conjugation and tendency to form aggregates results in red-edge tailing and a change in the simple binary spectral relationship [71]. As direct metric for the dimensions of the formed gels, we assessed irradiation-driven changes via SEC. Aliquots of P(MTC-*co*-PyChalEVE) were dissolved (18.3 mM PyChal (1.83 mM copolymer)) in DMAc and illuminated via blue (λ_{max} = 440 nm) and UV (λ_{max} = 310 nm) light and analyzed via

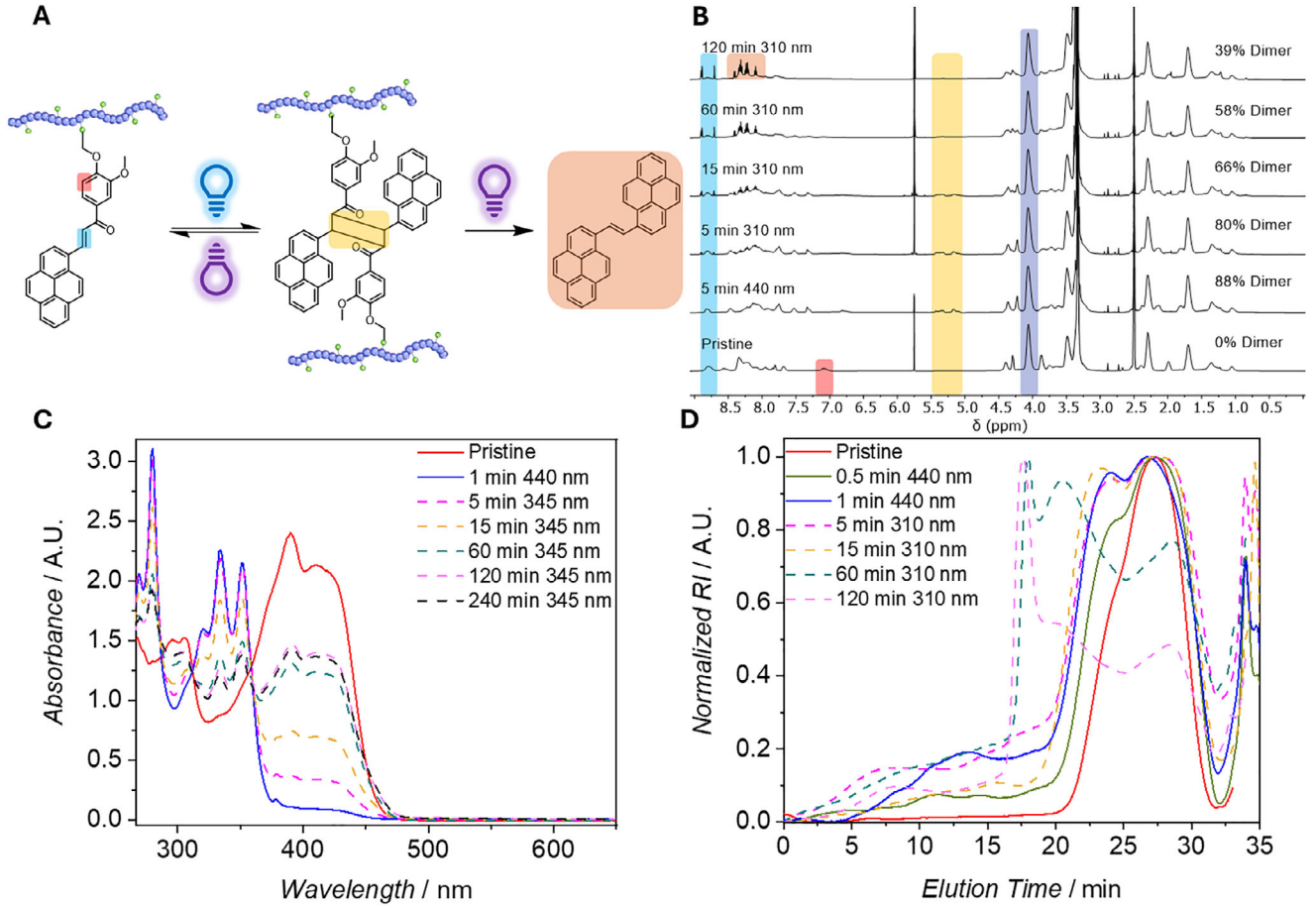

FIGURE 1 | Solution-state studies of the, (A) photocycloaddition/reversion of P(MTC-*co*-PyChalEVE) via blue and UV light LEDs, respectively, (B) chemical changes upon cycloaddition under 440 nm and reversion under 310 nm monitored via NMR spectroscopy (18.3 mM PyChal in DMSO-d_6), (C) evolution of the absorbance trace upon blue light (440 nm) and subsequent UV light (345 nm) irradiation screened via UV/Vis (18.3 mM PyChal in DMAc), and (D) elugram development under 440 and 310 nm light irradiation assessed via SEC (18.3 mM PyChal in DMAc), refer to the Supporting Information S1: Section 1.1 (Figure S1) for detailed emission spectra of the employed LEDs.

SEC (Figure 1D). Note that molar masses were obtained using a PMMA-based relative calibration and therefore represent values based on elution time that may not reflect the true sizes of the analyzed polymers (= apparent molar mass). Elution time (i.e., elution volume) is thus reported as the comparative metric. The pristine copolymer exhibited the previously noted unimodal elution trace. Brief irradiation at $\lambda_{max} = 440$ nm (0.5 min) resulted in an immediate redistribution of these populations (bold green trace in Figure 1D). Simultaneous shifts toward both lower and higher elution times were observed. The appearance of species with a higher hydrodynamic radius is attributed to intermolecular [2+2]-photocycloaddition-based cross-linking of PyChal units. In contrast, the concurrent increase in faster eluting species reflects competing intramolecular cross-linking towards single-chain nanoparticles, which could be expected in the applied dilute conditions [72]. Continued exposure to $\lambda_{max} = 440$ nm amplified the population at low elution time.

Upon subsequent exposure to UV light ($\lambda_{max} = 310$ nm), the chromatograms initially exhibited only minor changes but subsequently evolved toward increasingly shorter elution times after 60–120 min of irradiation, corresponding to larger apparent hydrodynamic radii of the structures. Owing to UV-induced photocycloreversion and the expected reduction in network connectivity, the opposite behavior was initially expected. Instead, the continued progression towards shorter elution times eventually approached elution times below 17 min, followed by an abrupt decrease in the recorded signal beyond this threshold (dashed traces in Figure 1D). Two effects may contribute to this unexpected behavior: (*i*) establishment of a photostationary state between PyChal dimerization and photocycloreversion, in which cross-link formation and cleavage proceed simultaneously and may transiently favor the formation of larger interconnected structures [73], and (*ii*) formation of hyperbranched or aggregated species following asymmetric photocycloreversion, which may exhibit non-ideal interactions with the stationary phase and thereby produce distorted elution profiles and an apparent increase of hydrodynamic size [74]. In particular, the asymmetric cleavage product bispyrene is expected to amplify this effect due to its limited solubility as well as its susceptibility for aggregation [75, 76]. Accordingly, the observed shift toward shorter elution times should be interpreted as an increase in apparent hydrodynamic volume rather than as direct evidence for an increase in the molar mass of the polymer.

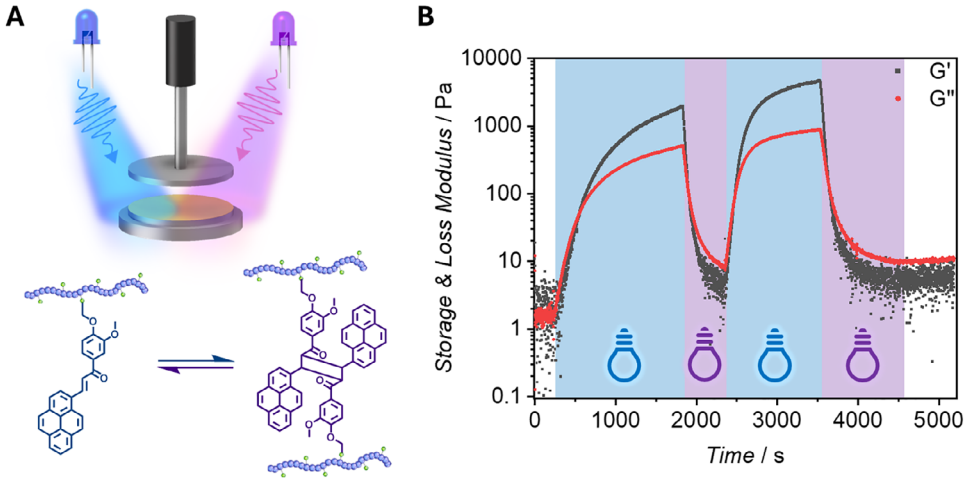

FIGURE 2 | (A) Small-amplitude oscillatory shear photorheology of P(MTC-*co*-PyChalEVE) transitioning reversibly from sols to gels and vice versa through different colors of light. (B) 30 wt.% Copolymer in DMSO: blue light irradiation (λ_{max} = 440 nm) induces gelation (G' ≈ 1.9 kPa after 20 min); UV light (λ_{max} = 335 nm) reverses the network (G' < 1 Pa within 5 min). Alternating irradiation cycles show reversible switching but an increased G′ after the second cycle (G' ≈ 4.7 kPa), refer to the Supporting Information S1: Section 1.1 (Figure S2) for detailed emission spectra of the utilized LEDs.

Having established the photochemistry of the PyChal-containing PCKA in solution, we translated this responsiveness into a gel system and monitored light-driven mechanical changes by small-amplitude oscillatory shear (SAOS) photorheology (Figure 2A). Photochemical cross-linking was examined at two polymer loadings (30 and 90 wt.% copolymer in DMSO) (Figure 2B and Figure S27). At 30 wt.%, pronounced gelation was observed under λ_{max} = 440 nm irradiation using an Omnicure S20 lamp. Within 20 min the storage modulus (G') increased to close to 1.9 kPa, surpassing G'', indicating a fast polymer cross-linking process. The gradual incline in G' value during the blue-induced cross-linking can be rationalized by the progressive restriction of polymer chain mobility upon gelation of the reaction mixture [77]. The color of light was then changed to λ_{max} = 340 nm causing rapid dissociation of the network: Within 5 min G' decreased to below G'' and fell below 10 Pa, indicating the transition to strongly viscous behavior. Repeated alternation of blue and UV irradiation demonstrated macroscopic reversibility of the mechanical response. After a second irradiation cycle, the post-gelation G' increased notably to close to 4.7 kPa (close to 2.5x the initial stiffness). We attribute this effect to secondary cross-linking from photooxidation under prolonged irradiation, as already observed by Koay et al. for a related PyChal-decorated PEG system [78]. We acknowledge that UV-induced cycloreversion of the networks resulted in substantial formation of low-molecular-weight photoproducts, rather than exclusively yielding bispyrene as the asymmetric cleavage product, as evidenced by solution-state ^{1}H-NMR and UV/Vis spectroscopy. This did, however, not affect the material's light-driven cyclability between the gel and sol states, as confirmed by photorheological measurements (Figure 1B,C and Figure 2B). When increasing the copolymer concentration to 90 wt.%, blue light-induced gelation proceeded more rapidly, attaining a $G'_{Plateau}$ of approx. 8.8 kPa after 8 min due to an increased chromophore density (refer to Figure S27). UV-induced dissociation was decisively slower, requiring 24 min to return to its initial viscous state. The storage modules obtained through light-induced cross-linking are generally substantially lower (approximately one order of magnitude) than those reported for PMTC networks synthesized by RROP directly, even after accounting for differences in solvent content and cross-linking density [79]. All materials of the present study are thus soft with G' in the low-kPa range, and remained amenable to spatiotemporal modulation, thereby significantly enhancing the range of materials available through CKA-based RROP [79, 80]. Network formation using blue light occurred more slowly than UV-induced reversion at 30 wt.% (with the reverse trend at 90 wt.%), which can be reasoned by a complex interplay of factors. These include intrinsic kinetics [81], quantum yields [82], percolation sensitivity of the forming network [83] as well as the presence of oxygen, that is, triplet state quenching, in addition to the already mentioned photooxidation (refer to Figure S28) [84]. The polymer loading dependence of the switching behavior supports an acceleration of the bimolecular kinetics of the [2+2]-photocycloaddition at high PyChal concentrations, whereas triplet state quenching may compromise the gelation rate under more dilute conditions. This relationship could be leveraged to fine-tune targeted material properties by modulating the probability and efficacy of cross-linking events and, consequently, the attainable material stiffness.

We subsequently exploited the underlying photochemistry together with the intrinsic degradability of PCKAs to fabricate microstructures by multi-photon lithography, followed by controlled, multimodal degradation of the printed objects (Figure 3). In contrast to conventional radical chain-growth polymerization, which accounts for the majority of established MPP photoresists, [2+2]-photocycloaddition represents a comparatively uncommon curing mechanism and exhibits fundamentally different requirements for efficient network formation [85]. In particular, the attainable curing efficiency in MPP depends on the two-photon absorption characteristics and photochemical quantum yield of the chromophore, as well as the spatial proximity and molecular organisation of the reactive groups. Accordingly, the photoresist formulation represents a critical parameter, as it must simultaneously provide sufficient concentrations of photoactive moieties for efficient network formation while maintaining adequate solubility of the polymer precursor and compatibility with the MPP process [86].

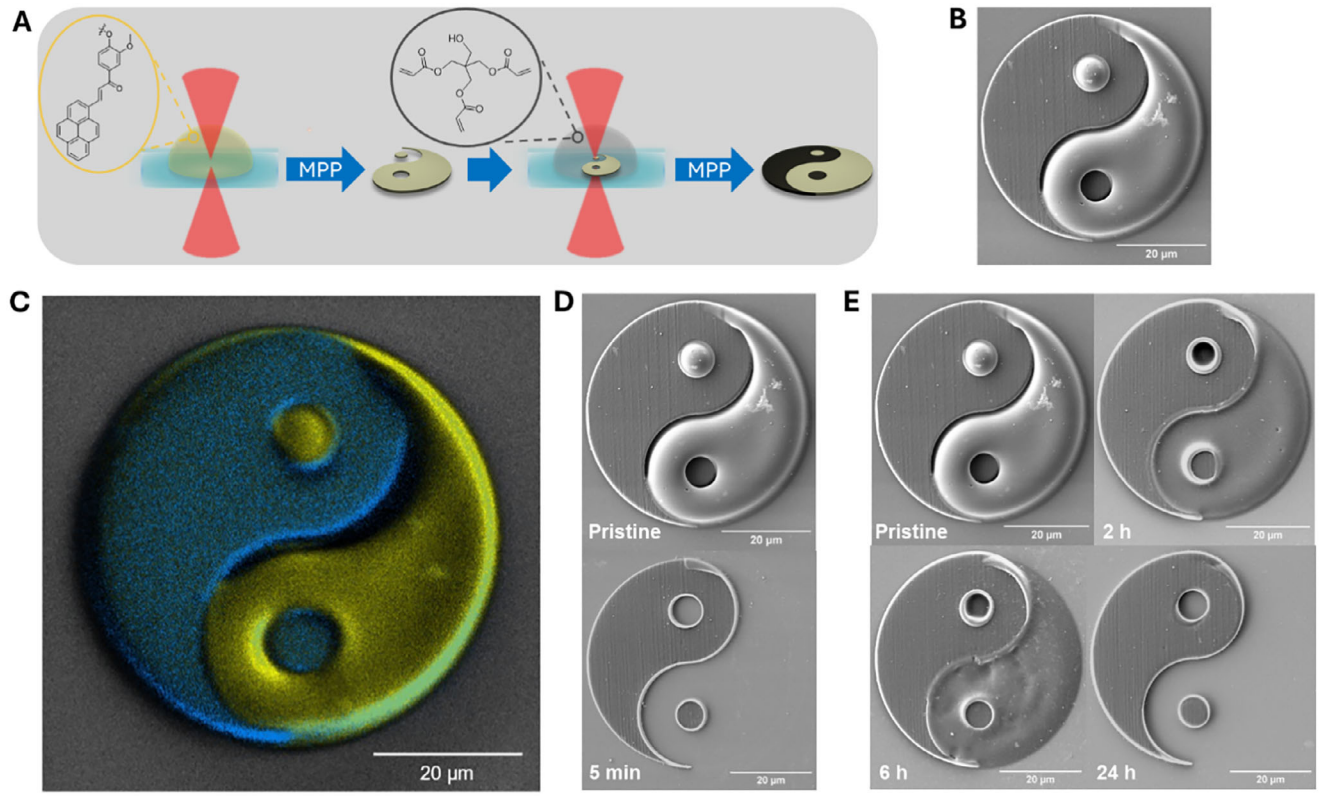

FIGURE 3 | (A) Sequential fabrication process of multi-material yin-yang structures via MPP. The yin part (tanwas printed from the PCKA-based resist (37.5 wt.% in ε-caprolactone, while the yang part (black) was printed from a commercial resist (Nanoscribe IP-S). (B) SEM image of the multi-material yin-yang print. (C) ToF-SIMS ion map, showing the overlaid intensities of fragments corresponding to $C_{4\text{-}16}H^-$ (yellow) and fragments corresponding to $C_{1\text{-}7}H_3O_{1\text{-}2}^-$ (blue) of the yang structure (a detailed list of individual fragments can be found in the Supporting Information S1: Section 1.4). (D) SEM array of the degradation of yin-yang microstructures in 0.05 M KOH in THF/MeOH, showcasing the pristine structure as well as after 5 min of exposure. (E) SEM array of the degradation of yin-yang multi-material objects in DMSO under irradiation with a 3 W LED (λ_{max} = 345 nm, refer to the Supporting Information S1: Section 1.1 (Figure S1) for a detailed emission spectrum of the utilized LED and to Supporting Information S1: Section 5.2.1 (Figure S32) for the degradation setup) showcasing the pristine structure and gradual decay after 2, 6, and 24 h.

Initial photoresin formulations comprising 25 wt.% P(MTC-*co*-PyChalEVE) in propylene carbonate/acetophenone provided a broad printability window. It was, however, associated with challenges in focusing the laser at the substrate-resin interface, the volatility of acetophenone despite its favorable solvent properties, and limited structural fidelity, prompting a transition to an alternative resin composition (refer to Figure S29). The printability window refers to the range of laser powers and scan speeds that yield continuous solidification, whereas structural fidelity denotes the accuracy and dimensional stability of the printed microstructures. Attempts to employ DMSO and DMF for MPP were hampered by rapid solvent evaporation and subsequent crystallization of the copolymer. PEG400 was also not feasible as it displayed insufficient copolymer solubilization capacity, with less than 25 wt.% copolymer dissolving. Cyrene, a greener alternative to DMF with a higher boiling point [87], provided an insufficient refractive index contrast relative to the borosilicate glass substrate ($\Delta n \leq 0.04$). Motivated by the recent study of van Durme et al., who employed ε-caprolactone as a non-volatile and chemically inert solvent for MPP, we adopted this solvent for our formulation [88]. A photoresist based on our photoreversible system was prepared by dissolving P(MTC-*co*-PyChalEVE) in ε-caprolactone without complementary additives and submitted to MPP. Specifically, we assessed the printability of the resist by fabricating cuboids via systematic variation of laser power and scanning speed in a so-called dose test. The herein employed PCKA resin exhibited an overall broad fabrication window across a broad range of laser powers and scanning speeds (refer to Figure S30), consistent with previous reports by Pashley-Johnson et al. who employed small molecules bearing telechelic PyChal moieties as chromophores in MPP [89]. Higher laser doses (effective exposure dose > $1.1025{\cdot}10^{-13}$ W^2s^2 m^{-1}) caused overexposure of the resist, resulting in reduced resolution and diminished feature definition due to microexplosions [90]. In contrast, underexposure of the resist resulted in poorly printed structures exhibiting no structural integrity due to a lack of cross-linking junctions. Such writing parameters not only critically affect the mechanical properties of the fabricated microstructures [91], but also the resolution of individual features. This is well documented in the literature and results from the influence of the laser power on the voxel size (volumetric pixel, which constitutes the smallest discrete 3D building block) [92, 93]. In addition, pronounced shrinkage of the printed structures was observed after development, likely due to network densification during polymerization and capillary stresses during solvent removal, with solvent evaporation during washing further exacerbating the process [94–96]. Despite the improved formulation, the printed features still exhibited limited structural fidelity and

substantial shrinkage during fabrication. To improve print resolution and structural integrity, the copolymer content within the ink was subsequently increased to 37.5 wt.%. Higher loadings of 50 wt.% resulted in only partial dissolution of the copolymer and thus produced an inhomogeneous ink incompatible with MPP. The higher copolymer loading now enabled the fabrication of 2.5D structures as test motifs in the scope of a practical demonstration format.

To demonstrate selective multi-material fabrication, yin-yang structures were fabricated with the yin part composed of our degradable PCKA resin and the yang part of a non-responsive acrylic resin (Nanoscribe, IP-S). The yin-yang geometry was chosen as a simple yet visually clear model system to show that our resist can retain its functionality after multi-photon fabrication, while enabling subsequent selective subtractive erasure. In practice, the multi-material structures were fabricated through a sequential two-resist MPP workflow. First, the yin structures were written using the PCKA-based resist (37.5 wt.% copolymer in *ε*-caprolactone), followed by development in DMSO to remove the unpolymerized resist and reveal the printed structures. Subsequently, the resulting yin structures were subjected to a second MPP step using the commercial IP-S photoresist to write the complementary yang structures. Development in acetone then removed the unpolymerized IP-S resist, yielding the final multi-material yin–yang structures. A dose test was carried out to optimize the printing parameters for the yin structures fabricated from our PCKA resist () (refer to Figure S31). Efficient printing was performed at a laser power of approximately 10 mW (20% of nominal 50 mW full power at the focal point) and a scanning speed of 4 mm s^{-1}. Under these conditions, all features remained well resolved, whereas higher doses caused pronounced overcuring, preventing reproducible patterned microfabrication. To understand structural homogeneity between both materials, a dose test was also performed for the IP-S resin and the thickness of both printed components was assessed by confocal microscopy. Based on these measurements, a laser power of approximately 17 mW and scanning speed of 5 mm s^{-1} was chosen for IP-S, providing homogeneous fabrication of both materials. The fabricated complementary 2.5D structure exhibited two optically distinguishable parts introduced by each resist (refer to Figure 3B). Differences in optical appearance likely arise from several factors, including the following: (*i*) The inherently slower kinetics of [2+2]-photocycloaddition of PyChal relative to radical chain-propagation of acrylic groups; (*ii*) The shrinkage of the PCKA structures stemming from polymer-chain entanglement and the increased spatial proximity induced by cyclobutane formation; and (*iii*) The higher dilution of the PCKA polymer in the resin, which increases the likelihood of intramolecular cross-linking events that do not contribute to the mechanical integrity of the printed object [86, 97, 98]. The chemical composition and spatial distribution of the fabricated microstructure were characterized via time-of-flight secondary-ion mass spectrometry (ToF-SIMS). ToF-SIMS images showed fragment ions attributable to pyrene ($C_{4\text{-}16}H^-$) were localized predominantly within the right yin (PCKA)-region (Figure 3C, plotted in yellow), whereas fragment ions characteristic of the acrylic resin ($C_{1\text{-}7}H_3O_{1\text{-}2}^-$) were collected in the left yang (IP-S) region (refer to Supporting Information S1: Section 1.4 for a comprehensive list of mapped ions, i.e. Tables S1 and S2).

As complete degradability is a hallmark characteristic of PCKA-derived materials, the decomposition behavior of the fabricated objects with a modular chemical structure was examined. In order to highlight the different and orthogonal degradation mechanism, accelerated hydrolysis of the PCKA-inherent ester linkages was performed under basic conditions and the disintegration of the $(PyChal)_2$ moieties was performed under UV-light (refer to Figure 3D,E, respectively). The degradability of MPP-fabricated PCKA structures had previously been demonstrated by Mattoli and co-workers, employing high cross-linker concentrations (>10 mol%) relative to the CKA content. Although this approach enabled the fabrication of intricate, high-fidelity microstructures through a radical chain-growth mechanism well established for high-resolution MPP, degradation of the resulting micro-objects required comparatively harsh conditions involving elevated acid/base concentrations and temperature [44]. In contrast, the present system combines a mechanistically distinct [2+2]-photocycloaddition-based network formation with a predominantly polyester backbone. The high content of hydrolytically labile ester linkages consequently enables chemical degradation under comparatively mild conditions, while the reversible PyChal cross-links provide an additional, orthogonal pathway for photochemical network disassembly. Taking advantage of the inherent susceptibility of the PCKA-derived ester bonds to undergo base-promoted hydrolysis, the developed structures were submerged in 0.05 M KOH in THF/MeOH (2:1, v/v) on glass substrates at ambient temperature. Degradation of the microstructures was monitored via scanning electron (SEM) and optical microscopy (Figure 3D,E). Under these conditions, complete disintegration of the PCKA structures occurred within 5 min, highlighting the pronounced susceptibility of the PCKA network towards basic cleavage. Notably, this brief degradation protocol, conducted at ambient temperature, is considerably milder than those reported previously. Our approach allows the selective degradation of the CKA backbone, while other ester bonds remain intact. Harsh basic conditions are known to also hydrolyze acrylate-based resists such as pentaerythritol triacrylate (PETA) [44, 99]. Structures printed from the non-responsive IP-S resist, which contains solely carbon-carbon bonds, showed little to no degradation under these conditions, confirming structure-dependent degradation (Figure 3D, bottom). In addition, PCKA-derived microstructures remained non-responsive in the absence of a base (refer to Figure S33).

We subsequently exploited the photoreversibility of the PyChal system by exposing the structures to LED irradiation at λ_{max} = 345 nm (I = 5.8 mW·cm^{-2}) in DMSO (refer to Figure S32 for the experimental setup). Photodegradation proceeded markedly more slowly (hours rather than minutes), allowing for a much more controlled disassembly over an extended timescale (Figure 3E). This behavior can be ascribed to three main factors: (*i*) Photocycloreversion occurs solely through cleavage of the cyclobutane-photodimer cross-links, rather than direct backbone scission; (*ii*) The limited penetration depth of UV light, governed by the density of absorbing moieties and compounded by the stronger absorption of shorter-wavelength radiation, which limits optical access and suggests a diffusion-limited process [93]; (*iii*) The spatial confinement of the degradative stimulus under unidirectional illumination (in contrast to the omnidirectional action of hydroxide ions) [93]. As a result, the progressive disappearance

of the structures with irradiation were followed over time (images taken after 2, 6, and 24 h). As with base-induced degradation, IP-S structures remained unaltered owing to the absence of photo-responsiveness, while sole PCKA-derived microstructures maintained their shape in the absence of light irradiation (refer to Figure S34). It is thus evident that the PCKA network enables a targeted erasure via two independent pathways.

3 | Conclusion

We herein demonstrate a key advancement of RROP of CKAs by integrating PMTC-based polyesters with mild reversible photochemistry to produce multifunctional, degradable polymer networks. A single-material platform is established that (*i*) is attainable through PPF of an existing PCKA backbone by installing PyChal pendants through CuAAC, (*ii*) exhibits wavelength-dependent [2+2]-photocycloaddition/photocycloreversion behavior in solution, (*iii*) shows photo-reversible modulation of network connectivity assessed via photorheology, (*iv*) can be processed by two-photon polymerization without additives to afford microstructures, and *(v)* can be erased by base and light, that is, by two orthogonal pathways. The resist's susceptibility to controlled degradation stimuli, that is, specific wavelengths and alkaline hydrolysis, enables targeted subtractive erasure that leaves other chemical moieties, i.e. the ones in the methacrylic IP-S resin, intact. Spatially resolved multi-material printing, confirmed by ToF-SIMS, further illustrates how RROP-derived polyester chemistry can be combined with photochemical selectivity to encode location-specific properties into printed architectures. Our study thus advances RROP by demonstrating initiator-free, MPP-processable PCKA resists and coupling reversible photochemistry directly to RROP-derived networks. We further highlight the need to balance monomer reactivity, radical ring-opening efficiency, pendant chromophore design and conjugation with the polyester backbone as well as cross-linking kinetics to achieve uniform networks with predictable/controlled degradation pathways. Future efforts will exploit complementary orthogonal (photo)chemistries to further diversify the attainable photochemical response of these materials. Simultaneously, the full potential of CKA chemistry will be realized through the inclusion of functional CKAs such as semi-crystalline, pH-sensitive or hydrophilic poly-CKAs, preserving a complete polyester architecture with programmable degradability. Such materials are anticipated to provide improved opportunities for enzymatic degradation under mild conditions. The convergence of these orthogonal CKA functionalities with photomodulation would establish a versatile class of sustainable, multifunctional soft materials capable of responding to multiple external stimuli while maintaining degradable network architectures [100]. Our results position photoadaptable networks based on RROP of CKAs as a versatile material platform for degradable soft matter for additive microfabrication as proof-of-concept functionality upon which application-oriented developments can be built.

Author Contributions

All authors have given approval to the final version of the manuscript. **Till Meissner**: performed conceptualization, formal analysis, investigation, data curation, writing – original draft, writing – review and editing, and visualization. **Julian Fanelli**: performed formal analysis, investigation, data curation, and writing – review and editing. **Vinh Xuan Truong**: performed formal analysis, investigation, data curation, and writing – review and editing. **Rob Jones**: performed formal analysis, investigation, data curation, and writing – review and editing. **Jens Gaitzsch**: performed conceptualisation, methodology, formal analysis, resources, data curation, writing – original draft, writing – review and editing, supervision, project administration, and funding acquisition. **Christopher Barner-Kowollik**: performed conceptualization, methodology, formal analysis, resources, data curation, writing – original draft, writing – review and editing, supervision, project administration, and funding acquisition.

Acknowledgements

J. G. acknowledges the German Research Foundation (DFG) for financial support as part of DFG project GA 2051/7-1. C.B.-K. acknowledges the Alexander-von-Humboldt Foundation for a Professorial Fellowship enabling his photochemical research program as well as the Materials Systems Engineering program of the Helmholtz Association. C.B.-K. further acknowledges the Deutsche Forschungsgemeinschaft (DFG, German Research Foundation) under Germany's Excellence Strategy for funding via the Excellence Cluster "3D Matter Made to Order" (EXC-2082/2-390761711), which is further supported by the State of Baden-Württemberg and by the Karlsruhe Institute of Technology (KIT). The authors acknowledge Elizabeth Graham, Drs. Yanan Xu and Lauren Geurds (all QUT) for photorheology discussions. The authors acknowledge A/Prof. Aaron Micallef (CARF at QUT) for performing and evaluating advanced NMR measurements. The authors acknowledge Dr. Jane Li (ANFF) for MPP assistance. The authors acknowledge John Griffin (CARF at QUT) for assistance with light microscopy. The authors acknowledge Dr. David Marshall (CARF at QUT) for the measurement and discussion of LC- and SEC-MS(/MS) experiments. The authors acknowledge Alicia Schmidt (QUT and KIT) for graphical design assistance. This work was enabled by use of the Central Analytical Research Facility (CARF) at the Queensland University of Technology (QUT) and by the Queensland node of the Australian National Fabrication Facility (ANFF), a company established under the National Collaborative Research Infrastructure Strategy to provide nano- and micro-fabrication facilities for Australia's researchers.

Open access publishing facilitated by Queensland University of Technology, as part of the Wiley - Queensland University of Technology agreement via the Council of Australasian University Librarians.

Conflicts of Interest

The authors declare no conflicts of interest.

Data Availability Statement

The data that support the findings of this study are available in the supplementary material of this article.

References

1. N. Ibrahim, A. M. N. A. A. Rahman, M. D. Shafiq, Z. Lockman, M. Jaafar, and Y. Kameda, "Microplastic Pollution: Sources, Degradation Mechanisms, Analytical Advances, And Mitigation Strategies For Environmental Sustainability," *Reviews of Environmental Contamination and Toxicology* 263 (2025): 27.

2. M. H. Stenzel, "The Dark Matter In Water, Air And Land: From Microplastic To Invisible Nanoplastics," *Materials Horizons* 13 (2026): 1628–1648.

3. P. J. Landrigan, S. Dunlop, M. Treskova, et al., "The Lancet Countdown on Health and Plastics," *Lancet* 406 (2025): 1044–1062.

4. C. V. Aarsen, A. Liguori, R. Mattsson, M. H. Sipponen, and M. Hakkarainen, "Designed to Degrade: Tailoring Polyesters for Circularity," *Chemical Reviews* 124 (2024): 8473–8515.

5. Y. Wang, R.-J. van Putten, A. Tietema, J. R. Parsons, and G.-J. M. Gruter, "Polyester biodegradability: Importance and Potential for Optimisation," *Green Chemistry* 26 (2024): 3698–3716.

6. C. Vilela, A. F. Sousa, A. C. Fonseca, et al., "The quest for Sustainable Polyesters – Insights Into The Future," *Polymer Chemistry* 5 (2014): 3119–3141.

7. E. Castro-Aguirre, F. Iñiguez-Franco, H. Samsudin, X. Fang, and R. Auras, "Poly(Lactic Acid)—Mass Production, Processing, Industrial Applications, And End Of Life," *Advanced Drug Delivery Reviews* 107 (2016): 333–366.

8. I. Vroman and L. Tighzert, "Biodegradable Polymers," *Materials* 2 (2009): 307–344.

9. A. W. Jackson, A. M. van Herk, and P. Thoniyot, "In Search of a Weak Link: Toward Biodegradability and Circular Economies Using Cyclic Ketene Acetals," *Industrial & Engineering Chemistry Research* 65 (2025): 34–46.

10. Y. Deng, A. Frezel, F. Mehner, P. Friedel, and J. Gaitzsch, "Amine-Bearing Cyclic Ketene Acetals for pH-Responsive And Degradable Polyesters Through Radical Ring-Opening Polymerisation," *Polymer Chemistry* 14 (2023): 4275–4281.

11. Y. Deng, J. Debbeler, A. Traeger, and J. Gaitzsch, "Degradable Nanocarriers Capable of Gene Delivery Derived from pH-Responsive Polyester: RROP Copolymerization Between Cyclic Ketene Acetals," *Macromolecular Rapid Communications* 47 (2026): 00722.

12. F. Mehner, M. Geisler, K. Arnhold, H. Komber, and J. Gaitzsch, "Structure–Property Relationships in Polyesters from UV-Initiated Radical Ring-Opening Polymerization of 2-Methylene-1,3-dioxepane (MDO)," *ACS Applied Polymer Materials* 4 (2022): 7891–7902.

13. W. J. Bailey, S.-R. Wu, and Z. Ni, "Synthesis and Free Radical Ring-Opening Polymerization of 2-Methylene-4-phenyl-1,3-dioxolane," *Die Makromolekulare Chemie* 183 (1982): 1913–1920.

14. M. R. Hill, E. Guégain, J. Tran, et al., "Radical Ring-Opening Copolymerization of Cyclic Ketene Acetals and Maleimides Affords Homogeneous Incorporation of Degradable Units," *ACS Macro Letters* 6 (2017): 1071–1077.

15. A. Tardy, J. Nicolas, D. Gigmes, C. Lefay, and Y. Guillaneuf, "Radical Ring-Opening Polymerization: Scope, Limitations, and Application to (Bio)Degradable Materials," *Chemical Reviews* 117 (2017): 1319–1406.

16. N. C. Jiang, Z. Zhou, and J. Niu, "Quantitative, Regiospecific, and Stereoselective Radical Ring-Opening Polymerization of Monosaccharide Cyclic Ketene Acetals," *Journal of the American Chemical Society* 146 (2024): 5056–5062.

17. J. Folini, W. Murad, F. Mehner, W. Meier, and J. Gaitzsch, "Updating Radical Ring-Opening Polymerisation of Cyclic Ketene Acetals From Synthesis To Degradation," *European Polymer Journal* 134 (2020): 109851.

18. J. Folini, C.-H. Huang, J. C. Anderson, W. P. Meier, and J. Gaitzsch, "Novel Monomers In Radical Ring-Opening Polymerisation For Biodegradable and pH Responsive Nanoparticles," *Polymer Chemistry* 10 (2019): 5285–5288.

19. C. Hardy, M. E. Levere, G. Kociok-Kohn, and A. Buchard, "Radical Ring Opening Polymerization of Cyclic Ketene Acetals Derived From D-Glucal," *ACS Macro Lett* 12 (2023): 1443–1449.

20. A. Kazama and Y. Kohsaka, "Radical Polymerization Of 'Dehydroaspirin' With The Formation Of A Hemiacetal Ester Skeleton: A Hint For Recyclable Vinyl Polymers," *Polymer Chemistry* 10 (2019): 2764–2768.

21. A. Kazama and Y. Kohsaka, "Diverse Chemically Recyclable Polymers Obtained By Cationic Vinyl And Ring-Opening Polymerizations Of The Cyclic Ketene Acetal Ester "Dehydroaspirin"," *Polymer Chemistry* 13 (2022): 6484–6491.

22. Y. Kohsaka, A. Kazama, K. Matsuo, S. Deguchi, and M. Osada, "Carbon-Resource Recovery from Vinyl Polymers of Cyclic Ketene Acetal Esters Using High-Temperature Water," *ACS Sustainable Resource Management* 1 (2024): 2234–2240.

23. Y. Kohsaka, H. Torisawa, and A. Kazama, "Synthesis and Polymerization Of Modified Dehydroaspirin With Increased Stability And Polymer Solubility," *Polymer Journal* 57 (2025): 1339–1346.

24. Y. Deng, F. Mehner, and J. Gaitzsch, "Current Standing on Radical Ring-Opening Polymerizations of Cyclic Ketene Acetals as Homopolymers and Copolymers with one another," *Macromolecular Rapid Communications* 44 (2023): 2200941.

25. T. Pesenti and J. Nicolas, "100th Anniversary of Macromolecular Science Viewpoint: Degradable Polymers from Radical Ring-Opening Polymerization: Latest Advances, New Directions, and Ongoing Challenges," *ACS Macro Letters* 9 (2020): 1812–1835.

26. F. Sbordone and H. Frisch, "Plenty of Space in the Backbone: Radical Ring-Opening Polymerization," *Chemistry–A European Journal* 30 (2024): 202401547.

27. E. Klemm and T. Schulze, "Ring-Opening Polymerization Of Heterocycles Bearing Substituted And Unsubstituted Exo-Methylene Groups - A Review," *Acta Polymerica* 50 (1999): 1–19.

28. G. G. Hedir, C. A. Bell, N. S. Ieong, et al., "Functional Degradable Polymers by Xanthate-Mediated Polymerization," *Macromolecules* 47 (2014): 2847–2852.

29. L.-F. Sun, R.-X. Zhuo, and Z.-L. Liu, "Studies on the Synthesis and Properties of Temperature Responsive and Biodegradable Hydrogels," *Macromolecular Bioscience* 3 (2003): 725–728.

30. A. Galperin, T. J. Long, and B. D. Ratner, "Degradable, Thermo-Sensitive Poly(N -isopropyl acrylamide)-Based Scaffolds with Controlled Porosity for Tissue Engineering Applications," *Biomacromolecules* 11 (2010): 2583–2592.

31. S. Komatsu, T. Sato, and A. Kikuchi, "Facile Preparation Of 2-Methylene-1,3-Dioxepane-Based Thermoresponsive Polymers And Hydrogels," *Polymer Journal* 53 (2021): 731–739.

32. Y. Shi, H. Schmalz, and S. Agarwal, "Designed Enzymatically Degradable Amphiphilic Conetworks by Radical Ring-Opening Polymerization," *Polymer Chemistry* 6 (2015): 6409–6415.

33. S. Louguet, V. Verret, L. Bédouet, et al., "Poly(Ethylene Glycol) Methacrylate Hydrolyzable Microspheres For Transient Vascular Embolization," *Acta Biomaterialia* 10 (2014): 1194–1205.

34. D. J. Siegwart, S. A. Bencherif, A. Srinivasan, J. O. Hollinger, and K. Matyjaszewski, "Synthesis, Characterization, And In Vitro Cell Culture Viability Of Degradable Poly(N -Isopropylacrylamide- co -5,6-benzo-2-methylene-1,3-dioxepane)-Based Polymers And Crosslinked Gels," *Journal of Biomedical Materials Research Part A* 87A (2008): 345–358.

35. Q. Jin, S. Maji, and S. Agarwal, "Novel Amphiphilic, Biodegradable, Biocompatible, Cross-Linkable Copolymers: Synthesis, Characterization and Drug Delivery Applications," *Polymer Chemistry* 3 (2012): 2785–2793.

36. A. Tardy, J. C. Honoré, J. Tran, et al., "Radical Copolymerization of Vinyl Ethers and Cyclic Ketene Acetals as a Versatile Platform to Design Functional Polyesters," *Angewandte Chemie International Edition* 56 (2017): 16515–16520.

37. Y. Shi, P. Zhou, V. Jérôme, R. Freitag, and S. Agarwal, "Enzymatically Degradable Polyester-Based Adhesives," *ACS Biomaterials Science & Engineering* 1 (2015): 971–977.

38. Y. Yang, K. Shi, K. Yu, et al., "Degradable Hydrogel Adhesives with Enhanced Tissue Adhesion, Superior Self-Healing, Cytocompatibility, and Antibacterial Property," *Advanced Healthcare Materials* 11 (2022): 2101504.

39. R. Yang, X. Zhang, B. Chen, Q. Yan, J. Yin, and S. Luan, "Tunable Backbone-Degradable Robust Tissue Adhesives Via In Situ Radical Ring-Opening Polymerization," *Nature Communications* 14 (2023): 6063.

40. X. Ai, J. Pan, Q. Xie, C. Ma, and G. Zhang, "UV-Curable Hyperbranched Poly(Ester- Co -Vinyl) By Radical Ring-Opening Copolymerization For Antifouling Coatings," *Polymer Chemistry* 12 (2021): 4524–4531.

41. G. Mu, J. Genzer, and C. B. Gorman, "Degradable Anti-Biofouling Polyester Coatings with Controllable Lifetimes," *Langmuir* 38 (2022): 1488–1496.

42. Q. Xie, Q. Xie, J. Pan, C. Ma, and G. Zhang, "Biodegradable Polymer with Hydrolysis-Induced Zwitterions for Antibiofouling," *ACS Applied Materials & Interfaces* 10 (2018): 11213–11220.

43. P. W. Kamm, L. L. Rodrigues, S. L. Walden, J. P. Blinco, A.-N. Unterreiner, and C. Barner-Kowollik, "Sequence-Independent Activation Of Photocycloadditions Using Two Colours Of Light," *Chemical Science* 13 (2022): 531–535.

44. M. Carlotti, O. Tricinci, and V. Mattoli, "Novel, High-Resolution, Subtractive Photoresist Formulations for 3D Direct Laser Writing Based on Cyclic Ketene Acetals," *Advanced Materials Technologies* 7 (2022): 2101590.

45. T. Meissner, P. Friedel, J. A. Carroll, C. Barner-Kowollik, and J. Gaitzsch, "Photochemical Action Plots Evidence UV-Promoted Radical Ring-Opening Polymerisation Of Cyclic Ketene Acetals," *Polymer Chemistry* 16 (2025): 704–711.

46. B. Luzel, S. Kouider, F. D'Agosto, et al., "Degradable Vinyl-Based Polymers by Radical Ring-Opening Polymerization: A User Guide," *ACS Polymers Au* 6 (2026): 721–785.

47. S. Maruo, O. Nakamura, and S. Kawata, "Three-Dimensional Microfabrication With Two-Photon-Absorbed Photopolymerization," *Optics Letters* 22 (1997): 132–134.

48. B. H. Cumpston, S. P. Ananthavel, S. Barlow, et al., "Two-Photon Polymerization Initiators For Three-Dimensional Optical Data Storage And Microfabrication," *Nature* 398 (1999): 51–54.

49. H. Frisch, D. E. Marschner, A. S. Goldmann, and C. Barner-Kowollik, "Wavelength-Gated Dynamic Covalent Chemistry," *Angewandte Chemie International Edition* 57 (2018): 2036–2045.

50. D. E. Marschner, H. Frisch, J. T. Offenloch, et al., "Visible Light [2 + 2] Cycloadditions for Reversible Polymer Ligation," *Macromolecules* 51 (2018): 3802–3807.

51. M. Van De Walle, K. De Bruycker, J. P. Blinco, and C. Barner-Kowollik, "Two Colour Photoflow Chemistry For Macromolecular Design," *Angewandte Chemie International Edition* 59 (2020): 14143–14147.

52. M. Van De Walle, C. Petit, J. P. Blinco, and C. Barner-Kowollik, "Visible-light reversible photopolymerisation: insights via online photoflow – electrospray ionisation – mass spectrometry," *Polymer Chemistry* 11 (2020): 6435–6440.

53. I. M. Irshadeen, K. De Bruycker, A. S. Micallef, S. L. Walden, H. Frisch, and C. Barner-Kowollik, "Green light LED Activated Ligation Of A Scalable, Versatile Chalcone Chromophore," *Polymer Chemistry* 12 (2021): 4903–4909.

54. K. Subramanian, V. Krishnasamy, S. Nanjundan, and A. V. Rami Reddy, "Photosensitive polymer: Synthesis, Characterization And Properties Of A Polymer Having Pendant Photocrosslinkable Group," *European Polymer Journal* 36 (2000): 2343–2350.

55. A. V. R. Reddy, K. Subramanian, V. Krishnasamy, and J. Ravichandran, "Synthesis, Characterization And Properties Of Novel Polymers Containing Pendant Photocrosslinkable Chalcone Moiety," *European Polymer Journal* 32 (1996): 919–926.

56. M. Tamilvanan, A. Pandurangan, K. Subramanian, and B. S. R. Reddy, "Synthesis and Characterization Of Mono- And Di-Methoxy Substituted Acrylate Polymers Containing Photocrosslinkable Pendant Chalcone Moiety," *Polymers for Advanced Technologies* 19 (2008): 1218–1225.

57. F. Biryan and G. Pihtili, "Fabrication of a Novel Acrylate Polymer Bearing Chalcone And Amide Groups And Investigation Of Its Thermal And Isoconversional Kinetic Analysis," *Journal of Thermal Analysis and Calorimetry* 139 (2020): 3857–3870.

58. T. Pesenti, E. Gillon, S. Ishii, et al., "Increasing the Hydrophilicity of Cyclic Ketene Acetals Improves the Hydrolytic Degradation of Vinyl Copolymers and the Interaction of Glycopolymer Nanoparticles with Lectins," *Biomacromolecules* 24 (2023): 991–1002.

59. M. Patel, "CuAAC And Beyond: A Review of Click Reaction Advances in Chemistry and Biology," *International Journal of Pharmaceutical Sciences* 3 (2025): 612–626.

60. E. Çalışkan, "Chemoselective Synthesis of Tyrosine-Based Polymers and Comparison of Their Thermal, Kinetic, and Dielectric Properties," *ChemistrySelect* 7 (2022): 202202010.

61. B. B. Nunez, B. Carbonnier, D. Grande, and B. L. Droumaguet, "Biporous Polycaprolactone-Like Networks From 2-Methylene-1,3-Dioxepane: A Versatile Platform Towards Functional And Reactive Polyesters," *Reactive and Functional Polymers* 214 (2025): 106284.

62. S. Jin and K. E. Gonsalves, "A Study of the Mechanism of the Free-Radical Ring-Opening Polymerization of 2-Methylene-1,3-dioxepane," *Macromolecules* 30 (1997): 3104–3106.

63. F. Mehner, T. Meissner, A. Seifert, A. Lederer, and J. Gaitzsch, "Kinetic Studies On The Radical Ring-Opening Polymerization Of 2-Methylene-1,3,6-Trioxocane," *Journal of Polymer Science* 61 (2023): 1882–1892.

64. F. Mehner, B. Hopkins, M. Reynolds-Green, D. J. Keddie, S. M. Howdle, and J. Gaitzsch, "Supercritical RROP: Exploring the Radical Ring-Opening Polymerisation of 2-Methylene-1,3,6-trioxocane in Supercritical CO_2 as a Green Solvent," *Polymer* 309 (2024): 127373.

65. E. Axioti, F. Mehner, M. Reynolds-Green, et al., "Nanoprecipitation and Drug Delivery with PMTC: Toward Biomedical Application of Polyesters from Radical Ring-Opening Polymerization," *Macromolecular Bioscience* 26 (2026): 00432.

66. J. Brandt, J. Lenz, K. Pahnke, F. G. Schmidt, C. Barner-Kowollik, and A. Lederer, "Investigation of Thermoreversible Polymer Networks By Temperature Dependent Size Exclusion Chromatography," *Polymer Chemistry* 8 (2017): 6598–6605.

67. J. Tran, T. Pesenti, J. Cressonnier, et al., "Degradable Copolymer Nanoparticles from Radical Ring-Opening Copolymerization between Cyclic Ketene Acetals and Vinyl Ethers," *Biomacromolecules* 20 (2019): 305–317.

68. J. A. Carroll, F. Pashley-Johnson, H. Frisch, and C. Barner-Kowollik, "Photochemical Action Plots Reveal Red-shifted Wavelength-dependent Photoproduct Distributions," *Chemistry–A European Journal* 30 (2024): 202304174.

69. M. Streicher, C.-H. Stamp, M. D. Kluth, A. Ripp, and C. Calvino, "Harnessing the Photoperformance of N -Methyl-Quinolinone for Gated Photo-Driven Cyclability and Reversible Photoligation," *Macromolecular Rapid Communications* 45 (2024): 2400474.

70. T. Guaratini, R. L. Vessecchi, F. C. Lavarda, et al., "New Chemical Evidence For The Ability To Generate Radical Molecular Ions Of Polyenes From ESI and HR-MALDI Mass Spectrometry," *Analyst* 129 (2004): 1223–1226.

71. W. Chen, N. B. Zuckerman, J. W. Lewis, J. P. Konopelski, and S. Chen, "Pyrene-Functionalized Ruthenium Nanoparticles: Novel Fluorescence Characteristics from Intraparticle Extended Conjugation," *Journal of Physical Chemistry C* 113 (2009): 16988–16995.

72. J. Willenbacher, K. N. R. Wuest, J. O. Mueller, M. Kaupp, H.-A. Wagenknecht, and C. Barner-Kowollik, "Photochemical Design of Functional Fluorescent Single-Chain Nanoparticles," *ACS Macro Letters* 3 (2014): 574–579.

73. L. C. Chambers, C. Barner-Kowollik, L. Barner, L. Michalek, and H. Frisch, "Photostationary State in Dynamic Covalent Networks," *ACS Macro Letters* 11 (2022): 532–536.

74. A. Khalyavina, L. Häußler, and A. Lederer, "Effect of the Degree Of Branching On The Glass Transition Temperature Of Polyesters," *Polymer* 53 (2012): 1049–1053.

75. L. Wang, W. Li, J. Lu, et al., "Supramolecular Nano-Aggregates Based on Bis(Pyrene) Derivatives for Lysosome-Targeted Cell Imaging," *Journal of Physical Chemistry C* 117 (2013): 26811–26820.

76. C. Huo, J.-C. Chambron, and M. Meyer, "Dual Emission Of A Bis (Pyrene)-Functionalized, Perbenzylated B-Cyclodextrin," *New Journal of Chemistry* 32 (2008): 1536–1542.

77. J.-Y. Yang, Y.-S. Kuk, B.-S. Kim, and M.-K. Seo, "Effects of Moisture Content and Heat Treatment on the Viscoelasticity and Gelation of Polyacrylonitrile/Dimethylsulfoxide Solutions," *Gels* 10 (2024): 728.

78. W. L. Koay, C. Gao, Q. T. Vu, et al., "Light Switchable Bioorthogonal Reaction Manifold for Modulation of Hydrogel Properties," *Biomacromolecules* 25 (2024): 6635–6644.

79. T. Meissner, S. Schäfer, C. Barner-Kowollik, S. Seiffert, and J. Gaitzsch, "Polyester Networks from Radical Ring-Opening Polymerization," *ACS Applied Polymer Materials* 7 (2025): 13936–13949.

80. T. Stirling and M. Zrínyi, "A Novel Method To Determine The Elastic Modulus Of Extremely Soft Materials," *Soft Matter* 11 (2015): 4180–4188.

81. C. Calvino, "Photocycloadditions for the Design of Reversible Photopolymerizations," *Chimia* 76 (2022): 816–825.

82. S. L. Walden, J. A. Carroll, A.-N. Unterreiner, and C. Barner-Kowollik, "Photochemical Action Plots Reveal the Fundamental Mismatch Between Absorptivity and Photochemical Reactivity," *Advanced Science* 11 (2024): 2306014.

83. J. H. Lee, R. K. Prud'homme, and I. A. Aksay, "Cure depth in photopolymerization: Experiments and theory," *Journal of Materials Research* 16 (2001): 3536–3544.

84. J.-T. Lin, H.-W. Liu, K.-T. Chen, and D.-C. Cheng, "Modeling the Kinetics, Curing Depth, and Efficacy of Radical-Mediated Photopolymerization: The Role Of Oxygen Inhibition, Viscosity, and Dynamic Light Intensity," *Frontiers in Chemistry* 13 (2019): 760.

85. S. C. Gauci, A. Vranic, E. Blasco, S. Bräse, M. Wegener, and C. Barner-Kowollik, "Photochemically Activated 3D Printing Inks: Current Status, Challenges, and Opportunities," *Advanced Materials* 36 (2024): 2306468.

86. A. Jaiswal, C. K. Rastogi, S. Rani, G. P. Singh, S. Saxena, and S. Shukla, "Two Decades Of Two-Photon Lithography: Materials Science Perspective For Additive Manufacturing of 2D/3D Nano-Microstructures," *iScience* 26 (2023): 106374.

87. J. Zhang, G. B. White, M. D. Ryan, A. J. Hunt, and M. J. Katz, "Dihydrolevoglucosenone (Cyrene) As a Green Alternative to N,N - Dimethylformamide (DMF) in MOF Synthesis," *ACS Sustainable Chemistry & Engineering* 4 (2016): 7186–7192.

88. B. Van Durme, A. Quaak, C. Vazquez Martel, et al., "Two-Photon Polymerized Poly (E-Caprolactone) Microstructures With Shape-Memory Behavior Under Compressive Loading," *Advanced Materials Technologies* 11 (2026): 02471.

89. F. Pashley-Johnson, R. Munaweera, S. I. Hossain, et al., "How Molecular Architecture Defines Quantum Yields," *Nature Communications* 15 (2024): 6033.

90. M. Tromayer, P. Gruber, A. Rosspeintner, et al., "Wavelength-optimized Two-Photon Polymerization Using Initiators Based on Multipolar Aminostyryl-1,3,5-triazines," *Scientific Reports* 8 (2018): 17273.

91. J. Bauer, A. Guell Izard, Y. Zhang, T. Baldacchini, and L. Valdevit, "Programmable Mechanical Properties of Two-Photon Polymerized Materials: From Nanowires to Bulk," *Advanced Materials Technologies* 4 (2019): 1900146.

92. X.-Z. Dong, Z.-S. Zhao, and X.-M. Duan, "Improving Spatial Resolution And Reducing Aspect Ratio In Multiphoton Polymerization Nanofabrication," *Applied Physics Letters* 92 (2008): 091113.

93. M. Gernhardt, V. X. Truong, and C. Barner-Kowollik, "Visible-Light-Degradable 3D Microstructures in Aqueous Environments," *Advanced Materials* 34 (2022): 2203474.

94. Y. Li, F. Qi, H. Yang, Q. Gong, X. Dong, and X. Duan, "Nonuniform Shrinkage And Stretching Of Polymerized Nanostructures Fabricated By Two-Photon Photopolymerization," *Nanotechnology* 19 (2008): 055303.

95. S. Maruo, T. Hasegawa, and N. Yoshimura, "Single-Anchor Support And Supercritical CO_2 Drying Enable High-Precision Microfabrication Of Three-Dimensional Structures," *Optics Express* 17 (2009): 20945–20951.

96. A. A. Bauhofer, S. Krödel, J. Rys, O. R. Bilal, A. Constantinescu, and C. Daraio, "Harnessing Photochemical Shrinkage in Direct Laser Writing for Shape Morphing of Polymer Sheets," *Advanced Materials* 29 (2017): 1703024.

97. A. Rehab, "New Photosensitive Polymers As Negative Photoresist Materials," *European Polymer Journal* 34 (1998): 1845–1855.

98. M. Formanek, L. Rovigatti, E. Zaccarelli, F. Sciortino, and A. J. Moreno, "Gel Formation in Reversibly Cross-Linking Polymers," *Macromolecules* 54 (2021): 6613–6627.

99. N. Hu, L. Ding, Y. Liu, et al., "Development of 3D-Printed Magnetic Micro-Nanorobots for Targeted Therapeutics: the State of Art," *Advanced NanoBiomed Research* 3 (2023): 2300018.

100. C. A. Spiegel, L. F. Martins, and E. Blasco, "Lighting the Future: 3D Printing Of Smart And Sustainable Materials," *Trends in Chemistry* 8 (2026): 162–176.

Supporting Information

Additional supporting information can be found online in the Supporting Information section.

Supporting File: adfm78296-sup-0001-SuppMat.pdf.